ACS OMEGA

Article

Cite This: ACS Omega 2019, 4, 1969−1981

http://pubs.acs.org/journal/acsodf

Initial Studies Directed toward the Rational Design of Aqueous Graphene Dispersants

Kane W. J. Heard,[†,⊥] Cian Bartlam,[‡] Christopher D. Williams,[∥] Junru Zhang,[†] Aula A. Alwattar,[†,§] Mark S. Little,[†] Adam V. S. Parry,[†] Fiona M. Porter,[†] Mark A. Vincent,[†] Ian H. Hillier,[†] Flor R. Siperstein,[∥] Aravind Vijayaraghavan,[‡] Stephen G. Yeates,*[,†] and Peter Quayle*[,†]

[†]School of Chemistry, The University of Manchester, Oxford Road, Manchester M13 9PL, U.K.

[‡]School of Materials and National Graphene Institute, The University of Manchester, Manchester M13 9PL, U.K.

[§]College of Science, University of Basrah, Garmat Ali, 61004 Basrah, Iraq

[∥]School of Chemical Engineering and Analytical Science, The University of Manchester, Oxford Road, Manchester M13 9PL, U.K.

Supporting Information

ABSTRACT: This study presents preliminary experimental data suggesting that sodium 4-(pyrene-1-yl)butane-1-sulfonate (PBSA), **5**, an analogue of sodium pyrene-1-sulfonate (PSA), **1**, enhances the stability of aqueous reduced graphene oxide (RGO) graphene dispersions. We find that RGO and exfoliated graphene dispersions prepared in the presence of **5** are approximately double the concentration of those made with commercially available PSA, **1**. Quantum mechanical and molecular dynamics simulations provide key insights into the behavior of these molecules on the graphene surface. The seemingly obvious introduction of a polar sulfonate head group linked via an appropriate alkyl spacer to the aromatic core results in both more efficient binding of **5** to the graphene surface and more efficient solvation of the polar head group by bulk solvent (water). Overall, this improves the stabilization of the graphene flakes by disfavoring dissociation of the stabilizer from the graphene surface and inhibiting reaggregation by electrostatic and steric repulsion. These insights are currently the subject of further investigations in an attempt to develop a rational approach to the design of more effective dispersing agents for rGO and graphene in aqueous solution.

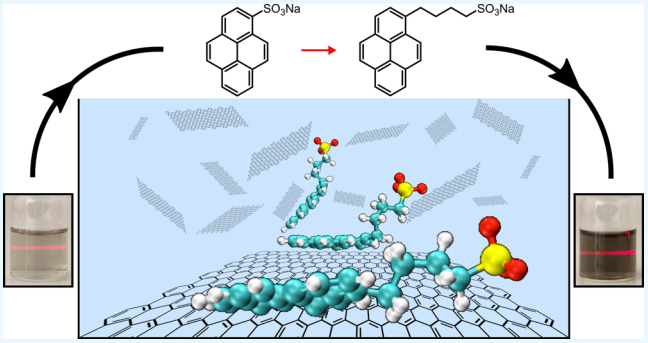

1. INTRODUCTION

It is now a truism that the isolation of graphene in 2004 has had an immeasurable effect upon materials science,[1,2] although a major hurdle, yet to be surmounted, is the development of scalable methods for its production. The most frequently employed preparation of graphene utilizes a "top-down" approach, which involves the direct exfoliation of bulk graphite into graphene flakes.[3−7] This can be achieved with the aid of mechanical forces[8,9] using sonication or shear mixing[10] in the liquid phase in order to overcome the strongly attractive interlayer van der Waals forces. More recently, the application of ball-milling[11] and electrochemical[12] techniques to graphene exfoliation has been expounded by a number of workers. The exfoliated graphene (EG) produced by these methods has properties that closely resemble "pristine" graphene, but there tends to be a mix of both single- and few-layer flakes in dispersion. In a slightly different approach, graphite is first oxidized, by one of a number of reagents, to graphite oxide, which then experiences interlayer expansion making graphite oxide more prone to solution-phase exfoliation, resulting in the production of high yields of graphene oxide (GO) monolayers.[13] The GO produced in such processes is a highly defective, insulating, two-dimensional (2D) material that disperses into polar solvents. The chemical or thermal reduction of the oxygen-containing functionality groups introduced in this exfoliation process reforms the lattice of sp^2-hybridized carbons, giving reduced GO (rGO) which has properties similar, but not identical, to that of "pristine" graphene.

The exact choice of a graphene material and processing conditions will ultimately depend on the final application to which the material is used, which dictates the specific properties that are required. Ideally, scalable production and processing requires stable, high-concentration dispersions, and in this regard, it has been shown that careful control of the surface tension and Hansen solubility parameters is crucial to finding a good solvent for graphene stability in solution.[14] Typically, the use of solvents such as *N*-methylpyrrolidin-2-one, *N*,*N*-dimethylformamide, or *ortho*-dichlorobenzene has found favor in the direct exfoliation of graphite because of their

Received: November 11, 2018
Accepted: December 14, 2018
Published: January 25, 2019

DOI: 10.1021/acsomega.8b03147
ACS Omega 2019, 4, 1969−1981

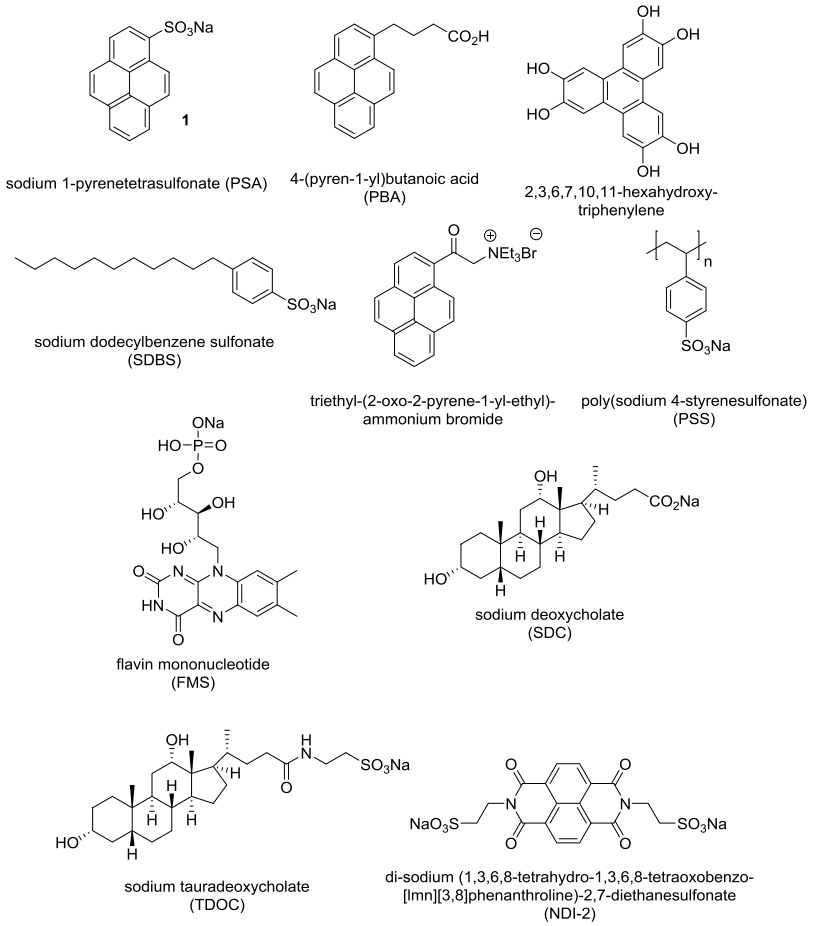

Figure 1. Representative stabilizers used in graphene exfoliation.[41]

ability to produce stable dispersions of EG and rGO. Unfortunately, the toxicity and high boiling points of these solvents will affect their acceptance in mass production and processing, whereas the use of environmentally benign solvents, such as water, is hampered by the generation of dispersions of low stability because of high surface tension and mismatched solubility parameters.[15,16]

The use of surfactants, polymers, and small organic molecules has also been investigated for exfoliation in aqueous media.[17−30] Unfortunately, any analysis of the compounds previously utilized for the stabilization of aqueous dispersions of rGO and EG is confused by the fact that these agents have been chosen on an empirical basis and include a broad range of structural motifs, which possess a diverse variety of functional groups. Many studies in this area have been, by necessity, driven pragmatically and frequently relied upon the use of commercially accessible materials, which were found to have stabilizing properties.[25−30] In the context of the present study, it is of interest to note therefore that Mohamed et al. (2016)[31] recently remarked that *advances* (in the optimization of the exfoliation process) *have been hampered by a lack of reliable predictive models for designing graphene-philic molecules because studies have been restricted to dispersing graphene using commercially available surfactants* and many of the stabilizers described in the literature may not therefore provide the optimal dispersion performance.[32] The evolution of a rational design process, more akin to that used in drug discovery, for the identification of more efficient exfoliants for 2D materials is problematical, as noted by Olivier and Samorì (2016),[33] because *a full understanding of the dispersion-stabilizing agent (DSA) role, needed for identifying the best DSAs to enhance the liquid-phase exfoliation (LPE) process, is still lacking.* This assessment was again recently echoed by Zhang et al. (2017)[34] when probing the use of 4-(pyrene-1-yl)butanoic acid (PBA), a commonly used intermediate[35,36] for the noncovalent functionalization of graphene, who concluded that *the nature of (the PBA) binding on graphene is poorly understood.* Indeed, the current state of the art has been most succinctly summarized by Coleman[37] who notes that *only a few systematic studies exist on the impact of the chemical structure of the surfactant on the degree of exfoliation and especially nanosheet size with little empirical data available apart from the most commonly used surfactants.* In conclusion, there are only limited reports on noncovalently stabilized aqueous graphene dispersions in the simulation literature,[38] and little work has been done on either the rationalization of stabilizer efficiency or the generation of a predictive model for the design of new stabilizers.[39] In this paper, we wish to present our initial findings concerning the development of a rational approach to the design and synthesis of aqueous graphene dispersing agents.

Any assessment of the exfoliation efficiency of a new stabilizer is complicated by the lack of standard experimental protocols for the exfoliation process itself and the use of poorly defined analytical regimens for determining the concentration of the exfoliated material.[40] Overall, these factors render it difficult to generate meaningful comparisons between newly engineered stabilizers with those previously reported in the

DOI: 10.1021/acsomega.8b03147
ACS Omega 2019, 4, 1969−1981

literature. That said, it is possible to make a number of gross generalizations concerning the structural features that are common to existing exfoliants/stabilizers, as embodied in the structures depicted in Figure 1, which has enabled the definition of a design strategy for the synthesis of more efficient stabilizing agents. Structural features that are common to many exfoliating agents that are reported in the literature include the following:

- The presence of a hydrophobic domain, oftentimes a polycyclic aromatic system, which is capable of entering into stabilizing $\pi-\pi$ interactions with the exfoliated material;
- The incorporation of reduced hydrocarbon fragments, such as those in a steroid nucleus or core structures decorated with long-chain hydrocarbon substructures, which may interact with the graphene surface via van der Waals forces;
- The presence of one or more polar/charged residues which disfavor aggregation of the exfoliated material because of unfavorable electrostatic and/or steric interactions. These polar functional groups (typically sulfonic acid salts, phenols, or ammonium salts) may also infer the solubility of the exfoliated material in polar solvents such as water.

2. RESULTS AND DISCUSSION

2.1. Molecular Design. The current research in this area reveals a central dichotomy: the direct exfoliation of graphite, which is well-suited to scale-up, is generally low yielding and produces a material with a lateral flake size of <1 μm because of the lack of control over cleavage and scission of graphite during sonication or shear mixing. The preparation of GO and rGO on the other hand results in the isolation of material possessing many defects because of the strong oxidation conditions during synthesis, although near quantitative conversions have been reported for these processes and lateral sizes of >100 μm are reported for GO.[2a] The reduction of GO to rGO is often carried out to restore graphitic properties to the material, be that electrical conductivity or superior mechanical properties for reinforcement in composites,[2b] or in the preparation of printable supercapacitors[2c] and solar cells,[2d] applications in which the control lateral flake size is particularly critical.

In this study, we sought to identify new stabilizers for the preparation of rGO and graphene flakes where structural and electronic features in the stabilizer could be modified in a systematic fashion, enabling a correlation between the structure and dispersion efficiency. In addition, this synthetic program would be supported by a theoretical study in which the structure-exfoliating efficiency could be probed in silico with a view to the development of a predictive model for the design of more efficient stabilizers. The starting point for our investigation was based upon the seminal investigation of Chen and Li[25,42] who first noted that sodium pyrene-1-sulfonate (PSA), **1**, was able to stabilize aqueous dispersions of graphene. Subsequent investigations by Green,[22] Feng and Müllen,[43] He,[44] and then Mullen and Casiraghi[45] provided further justification for the adoption of this and related substrates (e.g.,1-pyrenecarboxylic acid[30]) as graphene dispersing agents. Subsequent investigations by Casiraghi, Beljonne, and Palermo have also provided a theoretical understanding of the interaction between commercially available stabilizers such as PSA with graphene.[46] From these studies, it is now generally accepted that PSA which possesses an aromatic core (ca. 120 Å^2) participates in stabilizing $\pi-\pi$ interactions with the rGO and EG surface, and the polar, ionized, sulfonic acid head group ($ArSO_3\ominus$) enables both solvation by the bulk solvent (water) and the creation of a negatively charged adduct-flake surface, which results in electrostatic repulsion between flakes, thereby inhibiting reaggregation. However, we questioned whether the attachment of the bulky polar sulfonic acid residue, directly to the pyrene core, would in fact result in less than optimal $\pi-\pi$ interactions with the graphene surface and, potentially, a diminution in the degree of solvation by bulk water because of interactions of this moiety with the graphene surface.

In keeping with Liu's observations,[39] we hypothesized (Figure 2) that a simple structural modification to **1**, namely,

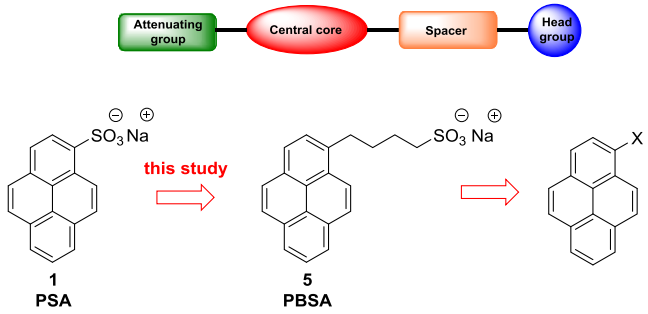

Figure 2. Design concept for the generation of new graphene stabilizing agents.

the introduction of a "spacer" between the polar head group ($RSO_3\ominus$) and the "central core", would generate a more efficient exfoliating agent, sodium 4-(pyrene-1-yl)butane-1-sulfonate (PBSA), on the premise that the conformationally mobile alkyl spacer would enable the pyrene core to achieve maximum $\pi-\pi$ interactions with the graphene surface as well as permit the polar sulfonic acid residue to be more exposed to the bulk solvent.[46] The introduction of a "spacer group" (e.g., an *n*-butyl chain) between the central core (pyrene) and the polar head group could also provide additional stabilization of the absorbed substrate by way of hydrophobic interactions. The choice of PBSA as a starting point for our initial investigations was, to some extent, a pragmatic decision and guided partly by the commercial availability of suitably prefunctionalized pyrene derivatives. Although similar strategies have been applied to the synthesis of new surfactants for the dispersion of carbon nanotubes,[47a−f] a systematic "QSAR"-type approach aimed at the development of new stabilizers for graphene exfoliation, which has not to our knowledge been used. In this approach, both the "spacer" and the electronic/steric properties of the central core could, in principle, be modified by the introduction of a range of "attenuating groups".[48] We considered that this model, in conjunction with relevant theoretical investigations, could enable the generation of a framework, in which the effect of substituent/core motifs on exfoliation efficiency could be addressed with the goal of achieving optimum exfoliation efficiency.

2.2. Synthesis. Having decided upon a design strategy (Figure 2), we embarked upon the synthesis of PBSA so that its efficiency as a stabilizing group in comparison with PSA could be determined. The synthesis of **5**[49,50] was accomplished

DOI: 10.1021/acsomega.8b03147
ACS Omega 2019, 4, 1969−1981

in a three-step sequence starting from 1-pyrenebutanoic acid, **2**, as outlined in Scheme 1.

Scheme 1. Synthesis of PBSA

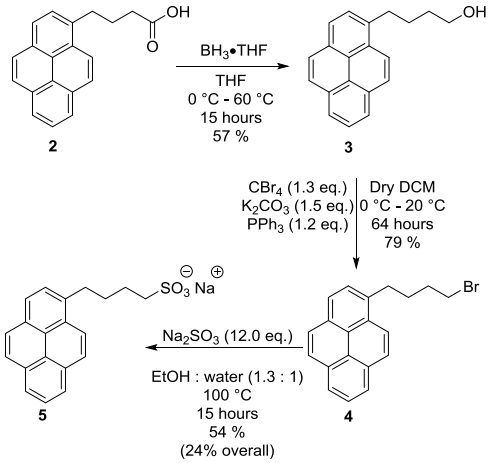

Reduction (BH_3·THF; 57%) of **2** to alcohol **3** followed by an Appel reaction[51] (PPh_3, 1.2 equiv; CBr_4, 1.3 equiv; K_2CO_3, 1.5 equiv; CH_2Cl_2; 79%) readily afforded bromide **4**. Finally, conversion of bromide **4** into **5** was accomplished by the reaction with an excess of sodium sulfite[52] (12 equiv) in aqueous ethanol at reflux. Removal of excess sodium sulfite proved feasible merely by washing the crude product with cold water. Finally, recrystallization of the triturated material from aqueous ethanol afforded PBSA in 54% yield; microanalytical and thermogravimetric analysis (TGA) data confirmed that this material was devoid of excess sulfite and was isolated as the monohydrate (see Experimental Procedures in the Supporting Information).

2.3. rGO Stabilization: Extinction Coefficient and Concentration. rGO was used for comparing the stabilization performance of PSA and PBSA because, in contrast with direct exfoliation of graphite, where the stabilizing molecule is closely responsible for the performance of the exfoliation as well as the stabilization of the EG flakes, this method solely concentrates on the stabilization of monolayer rGO. Graphite oxide was exfoliated, using a modified Hummers method,[53] to near 100% monolayer GO in water. By mixing this solution with a stabilizer and reducing the GO with L-ascorbic acid,[54] it was possible to probe the ability of the stabilizer at preventing reaggregation of the rGO flakes. For comparison, we developed an optimized general protocol for the preparation of rGO using the commercially available PSA and novel PBSA as stabilizers whereby both dispersions were subjected to the same processing conditions (see the Supporting Information). By varying the concentrations of both GO and the stabilizer molecule, we determined that a weight ratio of 3:1 PSA/GO (3 mg mL^{-1} PSA and 1 mg mL^{-1} GO) was found to give the optimum results for the commercial stabilizer in this protocol (see rGO/EG Methodology in the Supporting Information). This equates to 9.9 mM PSA and 8.3 MM PBSA. It was found that equal molar concentrations had little effect on the results (see the Supporting Information). It was also found during these preliminary experiments that sonication during the production process was necessary to produce dispersions of PSA-stabilized rGO because of partial reaggregation; therefore, this was included in the optimal processing conditions.

Raman spectroscopy and X-ray photoelectron spectroscopy (XPS) confirm the quality of the rGO flakes and that they are sufficiently reduced to reform the sp^2-hybridized network (Supporting Information). The I_D/I_G ratios of the PSA- and PBSA-stabilized rGO flakes are 1.43 and 1.51, respectively, which are comparable to other works, when accounting for a large D′ peak.[55] The C/O ratios, gained from peak-fitting the XPS C 1s spectra of GO and rGO, were 1.94 and 4.55, respectively. Peak fitting of the high-resolution C 1s spectra shows the return of a high level of carbon−carbon sp^2 bonding after reduction. By analyzing the lateral flake size by scanning electron microscopy (SEM), a reduction in lateral flake size is seen when compared to the GO dispersion, which is consistent with prolonged sonication and cleaning procedures.[56] The flake size distribution of the two stabilizers is comparable, demonstrating the robustness of this method. Analysis of atomic force microscopy (AFM) step height indicates that the majority of the flakes are monolayers, with no restacking of the flakes, with a thickness of approximately 1.5 nm, which is in agreement with literature values for monolayer rGO flakes with a monolayer of stabilizer molecules on each surface.[57] UV−vis spectroscopy was also employed in an attempt to quantify the concentration of the dispersed material and hence provides a measure of the stabilizing effect of **5** relative to **1**. It is possible to obtain a measure of the amount of graphene dispersed in a given sample by measuring the light attenuated at long wavelengths in the UV−vis spectra of these dispersions, where the higher concentrations of graphene result in a greater degree of light absorption.[58] By utilizing the absorption at 660 nm and normalizing with respect to the path length of the cuvette, a value of "Absorption-over-path length" ("Abs/*l*") can be obtained.[59] This comparison is only strictly reliable when, as in this case, the flake size and thickness are uniform throughout the samples and the light attenuation is only affected by the concentration and scattering effects are uniform across samples. We determine that the exfoliation of rGO with PBSA is comparable to the values reported in the literature for poly(sodium 4-styrenesulfonate)-stabilized rGO, where concentrations in the range of 0.1−1 mg mL^{-1} have been reported.[60] Weight concentrations are estimated to be 0.24 ± 0.07 and 0.60 ± 0.07 mg mL^{-1} for PSA and PBSA, respectively (Figure 3a), using an extinction coefficient of 5440 L g^{-1} m^{-1} at 660 nm,[61] which corresponds to an overall yield of approximately 60% for the PBSA-stabilized rGO. The increase in the concentration of the exfoliated material observed here may be ascribed to the greater stabilization proffered by PBSA toward rGO flake reaggregation, a result which is clearly evident to the naked eye (Figure 3a, inset). This assertion is supported by zeta potential (ζ) values[62] of −33 ± 2 and −40 ± 2 mV for PSA- and PBSA-stabilized rGO dispersions, respectively. These relative values do support the notion that PBSA appears to stabilize rGO more effectively than PSA. Ostensibly, this outcome may be due to a more efficient packing of PBSA on the surface of rGO when compared to that of PSA, where the conformationally mobile alkyl chain distances the polar head group from the anchoring pyrene moiety, which leads to a higher charge density on the surface of rGO, resulting in the inhibition of reaggregation. Irrespective of an incomplete understanding of the underlying reasons behind these results, the empirical observation that the simple homologation of PSA increases the exfoliation efficiency of rGO warranted further analysis, which led us to investigate graphite exfoliation using this agent.

DOI: 10.1021/acsomega.8b03147
ACS Omega 2019, 4, 1969−1981

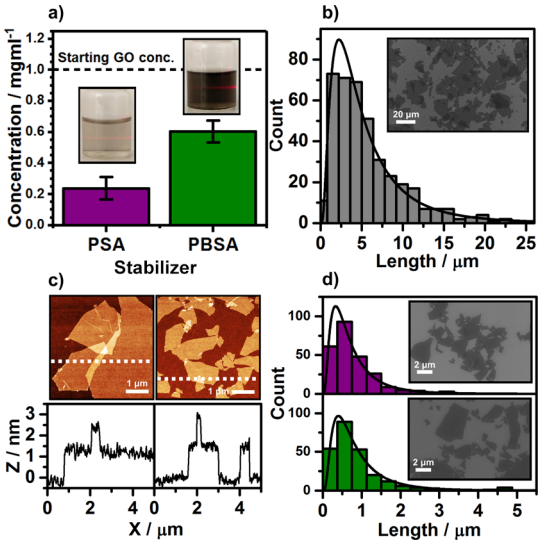

Figure 3. (a) Concentration values and standard deviation for rGO dispersions; the inset shows the photograph of the diluted dispersions, demonstrating the large increase in concentration using the PBSA stabilizer; (b) GO flake size distribution, before stabilization and reduction; (c) AFM of the stabilized rGO flakes dried on silicon dioxide showing large monolayer flakes with a thickness of approximately 1.5 nm from line scans; (d) flake size distribution for the stabilized and rGO for the stabilizers PSA and PBSA. The flake size has reduced from the starting GO dispersion as is expected after the washing procedures; both stabilizers show almost identical distributions.

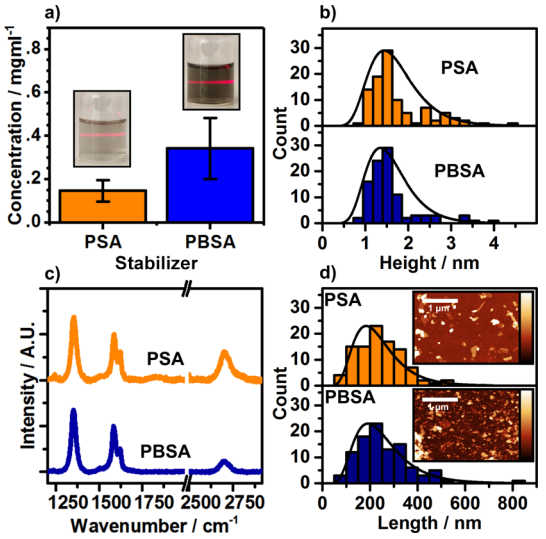

Figure 4. (a) Concentration values and standard deviation for EG and photographs of the diluted dispersions, where the increased concentration is evident using PBSA, whose results were consistent with those using rGO; (b) flake height (thickness) distribution from AFM analysis showing the majority of the flakes to be 1.5 nm thickness and containing monolayer, bilayer, and multilayer flakes. Both stabilizers show similar shape distributions; (c) Raman spectra for EG-stabilized dispersions; and (d) flake size distribution and AFM images (inset) for the graphene dispersions.

2.4. Direct Graphite Exfoliation. Preparing large quantities of graphene by the direct exfoliation of graphite into solution represents a major challenge.[63] Hence, we also determined the ability of PBSA to exfoliate and stabilize graphene by the LPE of graphite in water using tip sonication.[64] We modeled our study on the protocol developed by Green et al.[22] who noted that under optimized conditions, exfoliation of graphite in the presence of PSA (stabilizer/graphite = 1:30, w/w) afforded dispersions with a concentration of up to 3 mg mL^{-1}. A large excess of graphite is required in this process with upward of 95% not being exfoliated during sonication. In this protocol, each sample was tip-sonicated for 1 h and centrifuged to remove the residual insoluble graphitic material. The concentration for EG derived in this manner using PBSA was more than double that achieved using PSA, 0.34 ± 0.14 and 0.15 ± 0.05 mg mL^{-1} for PBSA and PSA, respectively (Figure 4a). Concentrations were determined by filtration, TGA, and the Beer−Lambert method to extract an extinction coefficient for both dispersions (see the Supporting Information for details). Extinction coefficients for the two dispersions were found to be 5917 and 5240 L g^{-1} m^{-1} at 660 nm for PBSA and PSA, respectively. These values are very similar to the latest results for exfoliated graphite dispersions cited in the literature and to that used in the rGO analysis discussed above.[65,66]

This result is very similar to that obtained for rGO, where again the increase in concentration is plainly evident merely by inspection with the naked eye (Figure 4, inset); however, unlike with rGO, the flake height and lateral flake size distribution is different (Figure 4b,d). Direct exfoliation of graphite does not produce solely monolayer graphene but instead gives a distribution of single, double, and multilayered flakes. Figure 4d shows that the flake size is different for the two stabilizers. Exfoliation with PBSA generates a broad distribution of flake sizes between 5 and 950 nm and a mean lateral flake size of 380 nm, whereas dispersion with PSA generates materials with a narrower flake size distribution between 5 and 450 nm with a mean size of 180 nm. This observation may suggest that either PBSA enhances the exfoliation process and allows for larger flakes to be mechanically sheared from the graphite or PBSA is able to stabilize larger flakes of EG in solution without reaggregation. The flake dimensions are further confirmed in the Raman spectra (Figure 4c).

Peak fitting of the 2D band in the Raman spectra (Supporting Information) shows few-layer graphene present in both samples when measured over 30 points. This is similar to that found in other works[17,45] and demonstrates that the EG concentration increase when using PBSA is not to the detriment of flake quality. The large D band in the Raman spectra of both PSA and PBSA dispersions (Figure 4c) can be attributed to all flakes being below the laser spot size used to analyze the samples (~0.5−1 μm), leading to a high contribution to the intensity from flake edges. This is further supported by the prominent D′ band in both spectra with both samples showing an $I_D/I_{D'}$ ratio of ~3, indicative of edge defects.[67] Zeta potential measurements for EG dispersions stabilized by PBSA have a larger negative zeta potential (−46 ± 1 mV) when compared to the PSA-stabilized dispersions (−41 ± 1 mV), which confirms a larger negative charge on the graphene surface, thereby enhancing the stabilization using this agent, in line with the results seen for rGO.

2.5. Computational Simulations. We have conducted a number of theoretical studies in order to provide a greater understanding of the binding of PSA and PBSA to the surface of graphene with the ultimate aim of defining those structural features, which may impart greater stabilizer efficiency. We have used quantum mechanical (QM) studies to focus on

DOI: 10.1021/acsomega.8b03147
ACS Omega 2019, 4, 1969−1981

electronic effects and classical molecular dynamical simulations, which permit a more thorough study of conformational effects (see the Supporting Information for full modeling procedures).

2.5.1. QM Studies. As the exfoliation efficiency of PSA and PBSA toward graphene was conducted in water, it was deemed important that any analysis of these processes, from a theoretical standpoint, must take solvation effects into account. We have previously shown that the semiempirical molecular orbital (MO) method corrected for dispersive interactions (PM6-DH2)[68] can predict both the adsorption energies of unsaturated hydrocarbons on graphene and the effect of substitution on these values to an accuracy comparable to density functional theory (DFT) values where these energies are in good agreement with the experimental determined values. The effect of bulk solvation can be included by means of the COSMO continuum model. Interaction energies (IEs) between PSA and PBSA with graphene (graphene sheet consisting of 1006 carbon atoms, end-capped with hydrogen) were therefore calculated at the PM6-DH2 level including solvation effects. In these studies, the polar sulfonate residues were explicitly solvated with three water molecules, where the hydrogen atoms of the water were directed toward the oxygen of the sulfonate residue, and the COSMO solvation model was then applied to the system as a whole. This analysis resulted in IEs of −111.3 and −123.8 kJ mol^{-1} for the deposition of PSA and PBSA, respectively, onto the model graphene surface. We suggest that the difference in IEs for these two substrates is due, in part, to hydrophobic effects. In the case of **5**, the *n*-butyl spacer is able to rest on the surface of the graphene in a manner reminiscent to that proposed by Groszek.[69] This QM analysis suggests that $\pi-\pi$ interactions dominate the binding of these molecules to the graphene, as the difference in binding energy between the two species is a modest 12.5 kJ mol^{-1} (i.e., 123.8−111.3 kJ mol^{-1}). Specifically, in the case of PBSA, this QM analysis suggests that in the bulk solution, the *n*-butyl spacer adopts an idealized, chain-extended, zigzag conformation (Figure 5a) similar to that observed for the single-crystal X-ray structure of PBA.[70] When PBSA approaches the surface of graphene, the *n*-butyl side chain adopts a new conformation[a], resulting in a stabilizing hydrophobic interaction between H(38), H(40), H(42), H(43), and H(44) and the graphene surface (Figure 5b). This conformational switch enables the polar head group to interact with the bulk solvent [C(20)−S(21) is projected at an angle of ca. 80° away from the basal plane of the pyrene core] where it appears that each oxygen of the sulfonate salt can enter into hydrogen bonding with the bulk solvent water. In the parent compound, PSA, a similar QM analysis (Supporting Information) indicates that two of the oxygen atoms of the sulfonate moiety are pointing either toward the surface of the graphene or parallel to it, leaving the third oxygen exposed to the bulk solvent (Figure 6).[33,71,72]

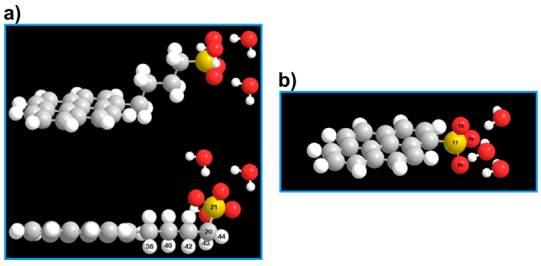

Figure 5. (a) Minimized structure of PBSA in bulk water (top) and that of PBSA adsorbed onto the surface of graphene using PM3-DH2 (bottom) and (b) minimized structure of PSA, 1, adsorbed onto the surface of graphene using PM3-DH2.

In summation, a QM analysis, which takes solvation into account, suggests that the introduction of a hydrophobic spacer group between the polar sulfonate residue and the pyrene core of PSA, leading to PBSA, generates a substrate with a higher IE with the surface of graphene, which, in principle, could translate into a more efficient stabilizer. Our QM approach generates structures that are similar to those generated by vdW-corrected DFT calculations for PBA adsorbed onto the surface of graphene[72] and provides a potentially useful model for the development of new stabilizers.[73]

2.5.2. Molecular Dynamics Simulations. Molecular dynamics (MD) simulations were also carried out in order to gain insights into the interactions between PSA and PBSA with a model graphene surface (see the Supporting Information for details) when placed in an aqueous environment. In the bulk solvent phase, these calculations indicate that PSA has a tendency for self-aggregation (Supporting Information, Figure S12a,b) behavior, which has been previously verified experimentally for **1**.[74,75] MD simulations were used to generate a potential of mean force (PMF) for the adsorption of PSA and PBSA onto a graphene surface in water showing that PBSA has a more favorable free energy of adsorption (−72.3 kJ mol^{-1}) than PSA (−52.5 kJ mol^{-1}), which can be primarily attributed to the additional carbons in the alkyl chain. Critically, PBSA has a slightly higher contribution to the overall energy from the aromatic core and a smaller energy associated with the sulfonate group (Supporting Information). The aliphatic carbons contribute to the overall free energy of adsorption, although individually they are only weakly interacting with the graphene surface.

MD simulations for PSA indicate that this molecule approaches the graphene surface along a "nose down" vector, in which the pyrene approaches on a trajectory that is orthogonal to the graphene surface and eventually adopts an equilibrium structure in which the pyrene ring system is approximately parallel to the basal plane of graphene. For PSA, the PMF (Figure 6a) has a minimum, point c, when the center of mass is at an equilibrium distance (z) of 0.38 nm from the graphene surface. The calculated average IE at this distance is −114.0 kJ mol^{-1}, of which −20.5 kJ mol^{-1} is derived from the interaction of the sulfonate head group with the graphene. These values are in remarkably close agreement with those previously calculated, with the total IE being remarkably close to our QM value (vide supra). As anticipated,[76] interaction of PSA with graphene generates a number of rapidly interconverting topologies in which the pyrene core of the dispersant is able to glide[72] along the surface of the graphene (Supporting Information, Figure S12 snapshots c−e). It should be noted that in the final averaged structure for PSA adsorbed onto the graphene surface, both O(18) and O(20) are directed toward the surface of the graphene, whereas O(19) is directed toward the bulk solvent. Torsion about C(16)−S(17) [C(7)−C(16)−C(17)−O(20) = −9.9°; C(7)−C(16)−S(17)−O(18) = 110.8°] reduces nonbonded interactions between the sulfonate residue and the pyrene ring, thus enabling the dipole associated with S(17)−O(19) to interact with the solvent

DOI: 10.1021/acsomega.8b03147
ACS Omega 2019, 4, 1969−1981

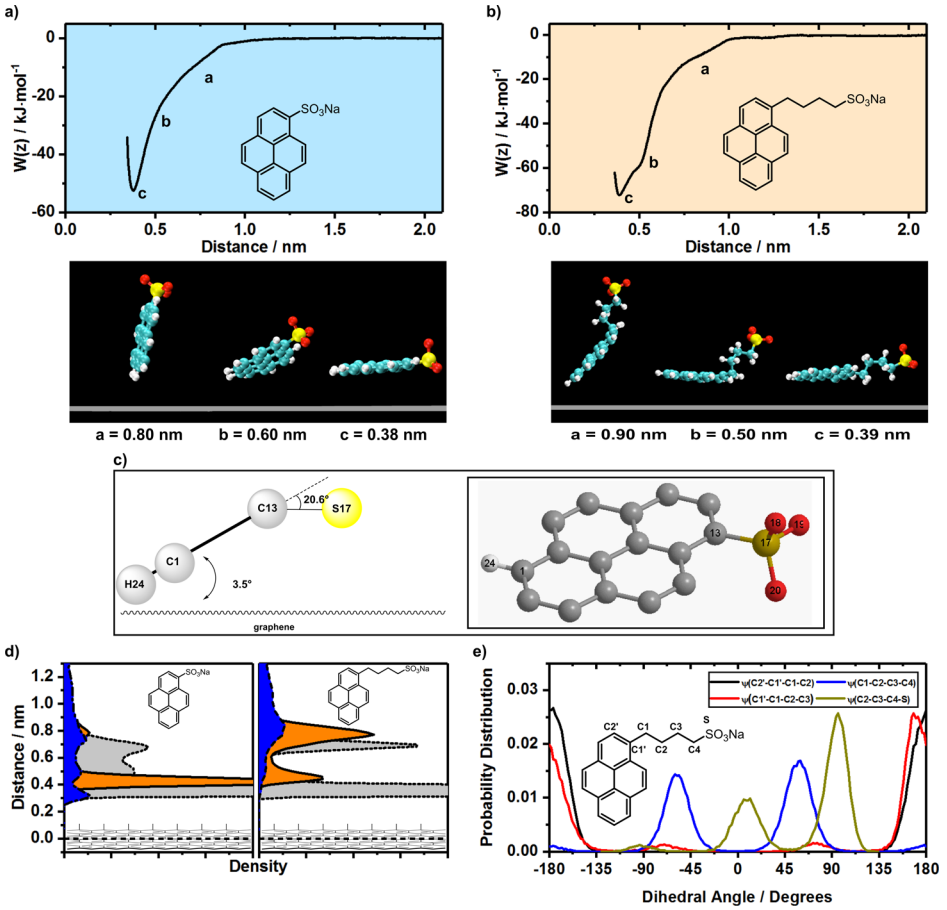

Figure 6. (a) Calculated PMF against the distance from the graphene sheet for PSA; (b) calculated PMF against the distance from the graphene sheet for PBSA with modeled molecular conformation at key stages of adsorption; (c) alignment of PSA to the surface of graphene; (d) plot of the number density, within the simulation box, of aromatic carbon (gray filled dotted line) sulfur (orange filled solid line) and sodium counterions (blue filled dashed line) as a function of distance from the graphene surface, located at 0 nm. This plot demonstrates that a high proportion of sulfur head groups and associated sodium counterions are found a significant distance away from the surface for PBSA as compared to that for PSA; (e) torsional data for PBSA when adsorbed onto the surface of graphene.

[C(7)−C(16)−S(17)−O(19) = −129.4]. The interaction of O(18) and O(20) with the graphene surface causes a distortion within the adsorbate molecule such that the C(16)−S(17) bond is bent away from the mean plane of the pyrene core by 20.6°. Interaction of the sulfonate residue with the graphene surface also forces the pyrene core to adopt a nonparallel alignment with the graphene surface, such that the mean plane containing the pyrene system has a tilt angle of 3.5° with respect to the graphene surface (Figure 6c). The fact that the pyrene core of PSA is not parallel to the graphene surface at the point of minimum energy, c, and that two of the oxygen atoms of the sulfonate group are pointing toward the graphene surface may result in less than the optimal $\pi-\pi$ interaction of the pyrene core with the graphene surface or solvation by the bulk solvent water. Indeed, it was this speculation that led us to prepare the substrate PBSA with a view to comparing its exfoliating efficiency with that of PSA.

In the case of PBSA, MD calculations suggest that in the bulk solvent, aggregation is again observed in a manner similar to that predicted for the aggregation of PBA prior to adsorption onto the surface of graphene (Supporting Information, Figure S13 snapshots a,b).[34] However, as PBSA approaches, the surface of the graphene deaggregation and then attachment to the surface are observed. As with PSA, PBSA is able to adopt a range of topologies with respect to the alignment of the pyrene core and the hexagonally packed carbon atoms of the graphene surface (Supporting Information, Figure S13c−e). The PMF for PBSA (Figure 6b) exhibits a minimum when the center of mass, z, is at a distance of 0.39 nm from the graphene surface (Figure 6b snapshot c). It is evident that the conformation adopted in snapshot c is not the same as the dominant conformation adopted in the bulk (snapshot a; z = 0.9 nm) or as PBSA approaching the surface of the graphene (snapshot b; z = 0.5 nm). The calculated average IE at 0.39 nm is −134.4 kJ mol^{-1}, of which −16.3 kJ mol^{-1} is derived from the interaction of the sulfonate head group with the graphene. In passing, it should be noted that the conformation adopted by the butyl side chain in PBSA in Figure 6 (snapshot c) is also similar to that proposed for the most stable conformation adopted by PBA when adsorbed onto the surface of graphene.[34,72]

This series of MD simulations also provides an analysis of density profiles of multiple stabilizer molecules interacting with a graphene surface. Figure 6d shows the density profiles for the aromatic carbons in the pyrene core, the sulfur atoms in the sulfonate groups, and the sodium counterions in the aqueous medium for both PSA and PBSA. These results suggest, as expected, that the aromatic core of both substrates is close to the graphene surface for both stabilizers (∼0.3 nm). For PSA (i.e., the stabilizer without the *n*-butyl chain), the majority of

DOI: 10.1021/acsomega.8b03147
ACS Omega 2019, 4, 1969−1981

the sulfonate groups reside in the same layer as the aromatic carbons, which is to be compared with PBSA in which a significant portion of the sulfur atoms is found at a distance of ≈0.8 nm from the graphene surface. In the case of PBSA, most of the sulfonate groups are located further above the graphene surface, which infers that the *n*-butyl side chain in PBSA points away from the graphene surface for higher stabilizer concentrations. The fact that the density of aromatic carbons close to the graphene surface is about 25% higher for PBSA when compared to PSA also infers that monolayer formation, rather than the stacking of the pyrene cores, is favored in such cases, which also has the net effect of increasing the concentration of negative charge on the graphene surface (as confirmed by zeta potential measurements) and hence increase the stability of the EG with respect to reaggregation.

An analysis of torsional data for the conformational preferences of the *n*-butyl spacer for adsorbed PBSA was also obtained for a single molecule of PBSA (see the Supporting Information). The results of this simulation are depicted in Figure 6e. Here, we observe that for a *single* PBSA molecule, the *n*-butyl spacer lies flat on the graphene surface, with a C(2′)−C(1′)−C(1)−C(2) torsion angle of ∼5°. At higher PBSA concentrations, there again appears to be a conformational switch such that the torsion angle about C(2′)−C(1′)−C(1)−C(2) becomes ∼90°. In this case, the alkyl side chain is orthogonal to the graphene surface with the sulfonate residue pointing into solution, thereby maximizing solvation by bulk water. We posit therefore that the conformational flexibility afforded by PBSA results in more efficient packing of the pyrene core, leading to a greater charge density on the graphene surface, which is reflected in the higher measured zeta potential for this system.

Taken together, these results infer therefore that in the case of PBSA, solvation of the $ArSO_3\ominus$ moiety by water competes favorably with any potential interaction of this moiety with the graphene surface. The possibility of additional stabilizing interactions between the C−H groups of the aliphatic chain of the stabilizer with the graphene surface is also maximized by the adoption of a chain-extended, zigzag conformation in which nonbonded interactions between vicinal CH_2 groups are minimized. The ability of PBSA to populate these configurations once bound to the graphene surface optimizes solvation of the polar sulfonate group, maximizes $\pi-\pi$ interactions, and facilitates the generation of additional stabilizing van der Waals interactions as well as prevents the reaggregation of the EG.

Although the theory described above and the experimental AFM data for the exfoliated data generated by PBSA are in accord with the "sandwich" structures that are commonly described in the literature for exfoliated rGO (i.e., a monolayer of stabilizer molecules attached to each surface of the exfoliated material[43,57]), it is by no means certain that our rather simplistic model leading to exfoliation is wholly accurate.[b] For example, it is possible that the dispersant used in the present study (PBSA), which may well aggregate in aqueous solution,[59,75] could generate bi- or multilayers[77] on the graphene surface or that PBSA could act as a molecular wedge during exfoliation.[72] A search of the literature reveals that many authors are circumspect concerning the nature of dispersant graphene aggregates, as has been recently noted by Bühlmann and co-workers,[78] who conclude that monolayer formation of the dispersant on the graphene surface is often assumed and not pursued rigorously. Of relevance to our investigation is that there is evidence for the formation of monolayers when pyrenebutyric acid, which is structurally similar to PBSA, is deposited onto the surface graphene.[34,79] It is clear however that additional studies, both in silico and in vitro, are required in order to derive a more fuller understanding of the exfoliation process, especially with respect to the aggregation state of the dispersant on the surface of the exfoliated material.

3. CONCLUSIONS

In this study, we present our initial findings directed toward the rational design of aqueous graphene dispersants. In this study, we demonstrate that PBSA (which is readily prepared from commercially available 1-pyrenebutanoic acid, **2**, in an operationally simple three-step synthesis) is a more efficient stabilizer of EG and rGO than commercially available PSA. In silico analysis of the binding of these molecules to the surface of graphene suggests that the addition of an *n*-butyl spacer between the pyrene core and the polar sulfonic acid residue allows the aromatic carbons of PBSA to lie parallel to, and bind more avidly with, the graphene surface, whereas the alkyl spacer has sufficient conformational freedom to direct the polar sulfonate residue into the bulk solvent. In contrast, binding of the commercially available stabilizer, PSA, to the surface of graphene forces the sulfonate group to interact with the graphene surface and lessens potential interaction with bulk water. We also suggest that the presence of the *n*-butyl chain in PBSA enables both more efficient packing of the stabilizer on the graphene surface and a lessened electrostatic repulsion[80] between adsorbed molecules on the surface of the graphene. Overall, this has the result of an increase in the zeta potential of the PBSA-dispersed material compared to that obtained with PSA, which increases its stability relative to the PSA-exfoliated material in solution. Having shown that a simple structural change can have an observable effect on the stabilizer efficiency and that these effects can be rationalized using computational methods, the development of a rational approach to stabilizer design and the mapping of the exfoliant once bound to the EG/rGO surface is now under active investigation.[81]

4. EXPERIMENTAL SECTION

4.1. Synthesis of PBSA. Full experimental details concerning the preparation of PBSA[49,50] can be found in the Supporting Information accompanying this paper.

4.2. rGO Dispersion Preparation. GO was prepared by a modified Hummers method whereby natural flake graphite (30 mesh, >96% C) was oxidized and exfoliated using H_2SO_4, $NaNO_3$, $KMnO_4$, and H_2O_2.[82] The resulting gel was repeatedly washed and exfoliated using a 3% wt H_2SO_4/0.5% wt H_2O_2 mixture and then brought to a pH of 7 using deionized (DI) water. The reduction of GO was performed in the presence of a stabilizer using L-ascorbic acid (Sigma-Aldrich) as the reducing agent. First, 60.0 mg of PSA (Sigma-Aldrich, **1**, 9.9 mM) or PBSA (**5**, 8.3 mM) was added to an aqueous dispersion of GO (1 mg mL^{-1}, 20 mL) and bath-sonicated (Elma P70H) for 30 min. Then, L-ascorbic acid (140.0 mg) was allowed to dissolve into the dispersion before being heated to 80 °C for 72 h. The mixture was subjected to bath sonication (15 min) and washed by centrifugation (Thermo Sorvall XTR, 15 000 rpm, 45 min) in order to remove the excess stabilizer. Here, 75% of the supernatant was removed

DOI: 10.1021/acsomega.8b03147
ACS Omega 2019, 4, 1969−1981

from the dispersion and replaced with an equivalent amount of DI water, followed by further sonication to redisperse the sediment. The sonication and washing steps were repeated 5 times, after which the dispersions were filtered through fine wool to remove any remaining aggregates. The filtered dispersions were used for all subsequent characterizations.

4.3. Production of Exfoliated Graphene. EG dispersions were prepared using probe sonication of graphite flakes. Initially, 18 mg of a pyrene stabilizer (PSA, 9.9 mM or PBSA, 8.3 mM) was added to 6 mL of DI water, heated, and stirred (85 °C, 10 min) to disperse the stabilizer. Each sample was then tip-sonicated in a 12 mL vial (tip depth ∼2 cm, Misonix Sonicator 3000, 24 W, 20 min) to ensure homogeneity. Flake graphite [30 mesh, >96% C, (540 mg)] was then added to the dispersion. The mixture was subjected to tip sonication for 1 h at 9 W, and an ice-water bath was used to maintain a low temperature. The mixture was then centrifuged (Eppendorf 5418 centrifuge, 5000 rpm, 1 h) to remove any unexfoliated graphite, and the supernatant was collected for further analysis.

4.4. Dispersion Characterization Techniques. Dispersions were spin-coated (3000 rpm) onto silicon substrates with 290 nm thermally grown SiO_2 for SEM, Raman, and AFM analyses. Flake size measurements were carried out on individual flakes using SEM micrographs (Zeiss Ultra Plus, InLens Detector), measuring 250 flakes along the same axis, and assuming a statistically random orientation of the flakes during sample preparation. Raman spectra were recorded using a Renishaw InVia spectrometer with a 514 nm laser at 1 mW power. The D and G peak intensities from the rGO Raman spectra were derived from peak fitting using a Gaussian/Lorentzian peak shape and deconvolution of the G peak accounting for a large D′. The EG Raman 2D peak fitting was carried out using multiple peaks with a full width at half-maximum of 24 cm^{-1}. AFM images were acquired using a Bruker instrument with a FastScan head and processed using WSxM. XPS of the starting GO powder and a nonstabilized washed rGO was carried out on a SPECS spectrometer. Zeta potential of dilute samples (approx. 100 times dilution) was measured using a Malvern Zetasizer NanoZS. Concentrations of the EG dispersions were estimated using UV−vis spectroscopy (Varian Cary 5000). Spectra were obtained for five dispersions diluted 30 times using a quartz cell with a path length of 1 mm. Absorbance at 660 nm was used to estimate the relative concentrations using absorbance over path length as described in the main text. Concentrations for the rGO dispersions were estimated using UV−vis spectroscopy (Thermo Genesys 10 s) with the machine set to measure at 660 nm, utilizing absorbance over path length. Three dispersions were measured using 10 mm path length quartz cells.

4.5. MD Simulations. MD simulations were carried out using the GROMACS software, version 5.0.4.[83] All simulations were performed in the canonical ensemble with the temperature maintained at 298 K using the Nosé−Hoover thermostat and a 1 ps relaxation time constant.[84,85] Equations of motion were integrated using the leapfrog algorithm with a time step of 1 fs. For the force field, the CHARMM[86−88] parameters were used to model graphene and the stabilizer molecules, the parameters of Joung and Cheatham[89] for Na^+ and TIP3P for water.[90] The graphene sheet was frozen in place for the duration of the simulations. Electrostatic interactions were accounted for using the particle mesh Ewald method,[91,92] and nonbonded interactions were cut off smoothly from 1.0 to 1.2 nm. For the PMF calculations, a graphene sheet was positioned at the bottom of a simulation cell with dimensions 3.7 nm × 3.8 nm × 5.0 nm. A stabilizer molecule was placed in the center of the cell, and the remainder was filled with water and one randomly positioned Na^+ counterion. The PMFs were calculated using an umbrella sampling procedure[93,94] and the weighted histogram analysis method.[95,96] In this procedure, the stabilizers were pulled onto the graphene sheet (at $z = 0$) using a harmonic potential with a force constant of 2500 kJ mol^{-1} nm^{-2} over 20 simulation windows from $z = 2.2−0.3$ nm. Each simulation was performed for 20 ns, and only the data from the final 19 ns were used to generate the PMF. An additional 10 ns simulation of the stabilizer adsorbed to the graphene sheet, without an umbrella potential, was carried out to obtain the IEs. In order to understand the orientation of the butyl spacer when PBSA is adsorbed, dihedral angle distributions were calculated from a 50 ns simulation, saving trajectory data for analysis every 1 ps to obtain smooth distributions. Higher concentrations of stabilizers were studied using a larger simulation cell (5.2 nm × 5.1 nm × 7.5 nm). An aqueous solution, consisting of 25 randomly distributed stabilizers 25 Na^+ counterions and 3600 water molecules, was positioned on the surface, leaving a 3.5 nm vacuum gap between the top of the solution and the bottom of the periodic image of the graphene sheet. All 25 stabilizer molecules were slowly pulled toward the surface at a rate of 0.002 nm ps^{-1}, using a harmonic potential with a force constant of 5000 kJ mol^{-1} nm^{-2} over 1.5 ns, followed by a 50 ns simulation in the absence of the harmonic potential. The data collected from the final 40 ns of this simulation were used to calculate the stabilizer density profiles.

4.6. QM Calculations. The QM calculations were carried using the PM6-DH2[97] approach as implemented in MOPAC2012.[98] PBSA was placed near the center of a 1006 carbon atom graphene sheet, terminated with 88 hydrogen atoms, with the sulfonate group solvated by three explicit water molecules. Bulk solvation effects of water were modeled by the COSMO approach employing a dielectric constant of 78.355. Geometry optimization was carried out on all structures and the energetics determined as the difference in energy of these optimized structures.

■ ASSOCIATED CONTENT

Supporting Information

The Supporting Information is available free of charge on the ACS Publications website at DOI: 10.1021/acsomega.8b03147.

Results of the MD simulations of PSA with the surface of graphene (MPG)

Results of the MD simulations of PBSA with the surface of graphene (MPG)

Full experimental details including NMR spectra of PBSA, characterization of stabilizer dispersions (UV−vis spectra, Raman, AFM, and high-resolution C 1s XPS spectra of GO/rGO), and details of the simulation studies (PDF)

■ AUTHOR INFORMATION

Corresponding Authors

*E-mail: stepehen.yeates@manchester.ac.uk (S.G.Y.).
*E-mail: peter.quayle@manchester.ac.uk (P.Q.).

DOI: 10.1021/acsomega.8b03147
ACS Omega 2019, 4, 1969−1981

ORCID

Kane W. J. Heard: 0000-0003-0002-9332
Christopher D. Williams: 0000-0002-5073-5924
Adam V. S. Parry: 0000-0001-9026-6088
Flor R. Siperstein: 0000-0003-3464-2100
Aravind Vijayaraghavan: 0000-0001-8289-2337
Peter Quayle: 0000-0002-0002-1894

Present Address

[⊥]Department of Chemistry, Imperial College, London SW7 2AY, UK.

Author Contributions

K.W.J.H., C.B., and M.S.L. contributed equally. The manuscript was written through contributions of all authors. All authors have given approval to the final version of the manuscript.

Notes

The authors declare no competing financial interest.

■ ACKNOWLEDGMENTS

We acknowledge the Engineering and Physical Sciences Research Council (EPSRC UK) for funding (EP/K03099X/1, EP/N010345/1, and EP/P027075/1). C.B. and A.V. acknowledge the EPSRC Industrial CASE Awards Scheme and Merck Chemicals Ltd., UK, for the financial support. K.W.J.H. thanks the EPSRC for the provision of a PhD studentship; F.M.P. thanks the EPSRC for the provision of a NOWANO PhD studentship. C.D.W. acknowledges the funding from the EPSRC (doctoral prize award EP/M506436/1); M.S.L. thanks the EPSRC for the provision of a predoctoral fellowship (EP/P505631/1). A.A.A. thanks the Iraqi Ministry of Higher Education and the University of Basrah (School of Chemistry) for the provision of a research scholarship. We also thank the University of Manchester for the use of the Computational Shared Facility (CSF). The University of Manchester thanks the EPSRC for the provision of Bruker NMR spectrometers (EP/K039547/1).

■ DEDICATION

Dedicated to the memory of Professor Paul O'Brien, FRS (1954−2018).

■ ADDITIONAL NOTES

[a]In solution, this arrangement, where the butyl spacer is *syn*-periplanar to the mean plane of the pyrene, is calculated to be 7.8 kJ mol^{-1} higher in energy than the conformation where the butyl spacer is orthogonal to the mean plane of the pyrene. [b]We thank a referee for invaluable discussion of this point.

■ REFERENCES

(1) Geim, A. K.; Novoselov, K. S. The Rise of Graphene. *Nat. Mater.* **2007**, *6*, 183−191.

(2) (a) Novoselov, K. S.; Fal'ko, V. I.; Colombo, L.; Gellert, P. R.; Schwab, M. G.; Kim, K. A Roadmap for Graphene. *Nature* **2012**, *490*, 192−200. (b) Tripathi, S. N.; Rao, G. S. S.; Mathur, A. B.; Jasra, R. Polyolefin/graphene nanocomposites: a review. *RSC Adv.* **2017**, *7*, 23615−23632. (c) Sun, J.; Cui, B.; Chu, F.; Yun, C.; He, M.; Li, L.; Song, Y. Printable Nanomaterials for the Fabrication of High-Performance Supercapacitors. *Nanomaterials* **2018**, *8*, 528. (d) Lee, S.; Yeo, J.-S.; Yun, J.-M.; Kim, D.-Y. Water Dispersion of Reduced Graphene Oxide Stabilized *via* Fullerenol Semiconductor for Organic Solar Cells. *Opt. Mat. Express* **2017**, *7*, 2487−2495.

(3) Lotya, M.; King, P. J.; Khan, U.; De, S.; Coleman, J. N. High-Concentration, Surfactant-Stabilized Graphene Dispersions. *ACS Nano* **2010**, *4*, 3155−3162.

(4) Paton, K. R.; Varrla, E.; Backes, C.; Smith, R. J.; Khan, U.; O'Neill, A.; Boland, C.; Lotya, M.; Istrate, O. M.; King, P.; Higgins, T.; Barwich, S.; May, P.; Puczkarski, P.; Ahmed, I.; Moebius, M.; Pettersson, H.; Long, E.; Coelho, J.; O'Brien, S. E.; McGuire, E. K.; Sanchez, B. M.; Duesberg, G. S.; McEvoy, N.; Pennycook, T. J.; Downing, C.; Crossley, A.; Nicolosi, V.; Coleman, J. N. Scalable Production of Large Quantities of Defect-Free Few-Layer Graphene by Shear Exfoliation in Liquids. *Nat. Mater.* **2014**, *13*, 624−630.

(5) Hernandez, Y.; Nicolosi, V.; Lotya, M.; Blighe, F. M.; Sun, Z.; De, S.; McGovern, I. T.; Holland, B.; Byrne, M.; Gun'Ko, Y. K.; Boland, J. J.; Niraj, P.; Duesberg, G.; Krishnamurthy, S.; Goodhue, R.; Hutchison, J.; Scardaci, V.; Ferrari, A. C.; Coleman, J. N. High-Yield Production of Graphene by Liquid-Phase Exfoliation of Graphite. *Nat. Nanotechnol.* **2008**, *3*, 563−568.

(6) Backes, C.; Szydłowska, B. M.; Harvey, A.; Yuan, S.; Vega-Mayoral, V.; Davies, B. R.; Zhao, P.-l.; Hanlon, D.; Santos, E. J. G.; Katsnelson, M. I.; Blau, W. J.; Gadermaier, C.; Coleman, J. N. Production of Highly Monolayer Enriched Dispersions of Liquid-Exfoliated Nanosheets by Liquid Cascade Centrifugation. *ACS Nano* **2016**, *10*, 1589−1601.

(7) Jawaid, A.; Nepal, D.; Park, K.; Jespersen, M.; Qualley, A.; Mirau, P.; Drummy, L. F.; Vaia, R. A. Mechanism for Liquid Phase Exfoliation of MoS2. *Chem. Mater.* **2015**, *28*, 337−348.

(8) Karagiannidis, P. G.; Hodge, S. A.; Lombardi, L.; Tomarchio, F.; Decorde, N.; Milana, S.; Goykhman, I.; Su, Y.; Mesite, S. V.; Johnstone, D. N.; Leary, R. K.; Midgley, P. A.; Pugno, N. M.; Torrisi, F.; Ferrari, A. C. Microfluidization of Graphite and Formulation of Graphene-Based Conductive Inks. *ACS Nano* **2017**, *11*, 2742−2755.

(9) Ciesielski, A.; Samorì, P. Graphene*via*sonication assisted liquid-phase exfoliation. *Chem. Soc. Rev.* **2014**, *43*, 381−398.

(10) Park, W. K.; Yoon, Y.; Song, Y. H.; Choi, S. Y.; Kim, S.; Do, Y.; Lee, J.; Park, H.; Yoon, D. H.; Yang, W. S. High-efficiency Exfoliation of Large-Area Mono-Layer Graphene Oxide with Controlled Dimension. *Sci. Rep.* **2017**, *7*, 16414.

(11) Buzaglo, M.; Bar, I. P.; Varenik, M.; Shunak, L.; Pevzner, S.; Regev, O. Graphite-to-Graphene: Total Conversion. *Adv. Mater.* **2016**, *29*, 1603528.

(12) Yang, S.; Ricciardulli, A. G.; Liu, S.; Dong, R.; Lohe, M. R.; Becker, A.; Squillaci, M. A.; Samorì, P.; Müllen, K.; Feng, X. Ultrafast Delamination of Graphite into High-Quality Graphene Using Alternating Currents. *Angew. Chem., Int. Ed.* **2017**, *56*, 6669−6675.

(13) Li, D.; Müller, M. B.; Gilje, S.; Kaner, R. B.; Wallace, G. G. Processable Aqueous Dispersions of Graphene Nanosheets. *Nat. Nanotechnol.* **2008**, *3*, 101−105.

(14) Hernandez, Y.; Lotya, M.; Rickard, D.; Bergin, S. D.; Coleman, J. N. Measurement of Multicomponent Solubility Parameters for Graphene Facilitates Solvent Discovery. *Langmuir* **2010**, *26*, 3208−3213.

(15) Backes, C.; Hauke, F.; Hirsch, A. The Potential of Perylene Bisimide Derivatives for the Solubilization of Carbon Nanotubes and Graphene. *Adv. Mater.* **2011**, *23*, 2588−2601.

(16) Salavagione, H. J.; Sherwood, J.; De bruyn, M.; Budarin, V. L.; Ellis, G. J.; Clark, J. H.; Shuttleworth, P. S. Identification of high performance solvents for the sustainable processing of graphene. *Green Chem.* **2017**, *19*, 2550−2560.

(17) Chabot, V.; Kim, B.; Sloper, B.; Tzoganakis, C.; Yu, A. High Yield Production and Purification of Few Layer Graphene by Gum Arabic Assisted Physical Sonication. *Sci. Rep.* **2013**, *3*, 1378.

(18) Wang, M.; Niu, Y.; Zhou, J.; Wen, H.; Zhang, Z.; Luo, D.; Gao, D.; Yang, J.; Liang, D.; Li, Y. The Dispersion and Aggregation of Graphene Oxide in Aqueous Media. *Nanoscale* **2016**, *8*, 14587−14592.

(19) Ye, Y.-S.; Zeng, H.-X.; Wu, J.; Dong, L.-Y.; Zhu, J.-T.; Xue, Z.-G.; Zhou, X.-P.; Xie, X.-L.; Mai, Y.-W. Biocompatible Reduced Graphene Oxide Sheets with Superior Water Dispersibility Stabilized

DOI: 10.1021/acsomega.8b03147
ACS Omega 2019, 4, 1969−1981

by Cellulose Nanocrystals and Their Polyethylene Oxide Composites. *Green Chem.* **2016**, *18*, 1674−1683.
(20) McManus, D.; Vranic, S.; Withers, F.; Sanchez-Romaguera, V.; Macucci, M.; Yang, H.; Sorrentino, R.; Parvez, K.; Son, S.-K.; Iannaccone, G.; Kostarelos, K.; Fiori, G.; Casiraghi, C. Water-Based and Biocompatible 2D Crystal Inks for All-Inkjet-Printed Heterostructures. *Nat. Nanotechnol.* **2017**, *12*, 343−350.
(21) Robinson, B. J.; Bailey, S. W. D.; O'Driscoll, L. J.; Visontai, D.; Welsh, D. J.; Mostert, A. B.; Mazzocco, R.; Rabot, C.; Jarvis, S. P.; Kolosov, O. V.; Bryce, M. R.; Lambert, C. Formation of Two-Dimensional Micelles on Graphene: Multi-Scale Theoretical and Experimental Study. *ACS Nano* **2017**, *11*, 3404−3412.
(22) Parviz, D.; Das, S.; Ahmed, H. S. T.; Irin, F.; Bhattacharia, S.; Green, M. J. Dispersions of Non-Covalently Functionalized Graphene with Minimal Stabilizer. *ACS Nano* **2012**, *6*, 8857−8867.
(23) Narayan, R.; Lim, J.; Jeon, T.; Li, D. J.; Kim, S. O. Perylene Tetracarboxylate Surfactant Assisted Liquid Phase Exfoliation of Graphite into Graphene Nanosheets with Facile Re-Dispersibility in Aqueous/organic Polar Solvents. *Carbon* **2017**, *119*, 555−568.
(24) Guardia, L.; Fernández-Merino, M. J.; Paredes, J. I.; Solís-Fernández, P.; Villar-Rodil, S.; Martínez-Alonso, A.; Tascón, J. M. D. High-Throughput Production of Pristine Graphene in an Aqueous Dispersion Assisted by Non-Ionic Surfactants. *Carbon* **2011**, *49*, 1653−1662.
(25) Wang, H.; Xia, B.; Yan, Y.; Li, N.; Wang, J.-Y.; Wang, X. Water-Soluble Polymer Exfoliated Graphene: As Catalyst Support and Sensor. *J. Phys. Chem. B* **2013**, *117*, 5606−5613.
(26) Caridad, B.; Paredes, J. I.; Pérez-Vidal, O.; Villar-Rodil, S.; Pagán, A.; Cenis, J. L.; Martínez-Alonso, A. A Biosupramolecular Approach to Graphene: Complementary Nucleotide-Nucleobase Combinations as Enhanced Stabilizers Towards Aqueous-Phase Exfoliation and Functional Graphene-Nucleotide Hydrogels. *Carbon* **2018**, *129*, 321−334.
(27) Lotya, M.; Hernandez, Y.; King, P. J.; Smith, R. J.; Nicolosi, V.; Karlsson, L. S.; Blighe, F. M.; De, S.; Wang, Z.; McGovern, I. T.; Duesburg, G. S.; Duesberg, G. S. Liquid Phase Production of Graphene by Exfoliation of Graphite in Surfactant/Water Solutions. *J. Am. Chem. Soc.* **2009**, *131*, 3611−3620.
(28) Arao, Y.; Kubouchi, M. High-Rate Production of Few-Layer Graphene by High-Power Probe Sonication. *Carbon* **2015**, *95*, 802−808.
(29) He, P.; Sun, J.; Tian, S.; Yang, S.; Ding, S.; Ding, G.; Xie, X.; Jiang, M. Processable Aqueous Dispersions of Graphene Stabilized by Graphene Quantum Dots. *Chem. Mater.* **2014**, *27*, 218−226.
(30) An, X.; Simmons, T.; Shah, R.; Wolfe, C.; Lewis, K. M.; Washington, M.; Nayak, S. K.; Talapatra, S.; Kar, S. Stable Aqueous Dispersions of Noncovalently Functionalized Graphene from Graphite and their Multifunctional High-Performance Applications. *Nano Lett.* **2010**, *10*, 4295−4301.
(31) Mohamed, A.; Ardyani, T.; Bakar, S. A.; Brown, P.; Hollamby, M.; Sagisaka, M.; Eastoe, J. Graphene-Philic Surfactants for Nanocomposites in Latex Technology. *Adv. Colloid Interface Sci.* **2016**, *230*, 54−69.
(32) Lin, S.; Shih, C.-J.; Sresht, V.; Rajan, A. V.; Strano, M. S.; Blankschtein, D. Understanding the colloidal dispersion stability of 1D and 2D materials: Perspectives from molecular simulations and theoretical modeling. *Adv. Colloid Interface Sci.* **2017**, *244*, 36−53.
(33) Haar, S.; Bruna, M.; Lian, J. X.; Tomarchio, F.; Olivier, Y.; Mazzaro, R.; Morandi, V.; Moran, J.; Ferrari, A. C.; Beljonne, D.; Ciesielski, A.; Samorì, P. Liquid-Phase Exfoliation of Graphite into Single- and Few-Layer Graphene with α-Functionalized Alkanes. *J. Phys. Chem. Lett.* **2016**, *7*, 2714−2721.
(34) Hinnemo, M.; Zhao, J.; Ahlberg, P.; Hägglund, C.; Djurberg, V.; Scheicher, R. H.; Zhang, S.-L.; Zhang, Z.-B. On Monolayer Formation of Pyrenebutyric Acid on Graphene. *Langmuir* **2017**, *33*, 3588−3593.
(35) Seo, S.; Hwang, E.; Cho, Y.; Lee, J.; Lee, H. Functional Molecular Junctions Derived from Double Self-Assembled Monolayers. *Angew. Chem., Int. Ed.* **2017**, *56*, 12122−12126.
(36) Wu, G.; Tang, X.; Meyyappan, M.; Lai, K. W. C. Doping Effects of Surface Functionalization on Graphene with Aromatic Molecule and Organic Solvents. *Appl. Surf. Sci.* **2017**, *425*, 713−721.
(37) Backes, C.; Higgins, T. M.; Kelly, A.; Boland, C.; Harvey, A.; Hanlon, D.; Coleman, J. N. Guidelines for Exfoliation, Characterization and Processing of Layered Materials Produced by Liquid Exfoliation. *Chem. Mater.* **2016**, *29*, 243−255.
(38) Kulkarni, A.; Mukhopadhyay, N.; Bhattacharyya, A. R.; Panwar, A. S. Dispersion of Non-Covalently Modified Graphene in Aqueous Medium: A Molecular Dynamics Simulation Approach. *RSC Adv.* **2017**, *7*, 4460−4467.
(39) Zhang, L.; Zhang, Z.; He, C.; Dai, L.; Liu, J.; Wang, L. Rationally Designed Surfactants for Few-Layered Graphene Exfoliation: Ionic Groups Attached to Electron-Deficient π-Conjugated Unit through Alkyl Spacers. *ACS Nano* **2014**, *8*, 6663−6670.
(40) For a discussion see: Paton, K. R.; Coleman, J. N. Relating the Optical Absorption Coefficient of Nanosheet Dispersions to the Intrinsic Monolayer Absorption. *Carbon* **2016**, *107*, 733−738.
(41) Fernández-Merino, M. J.; Paredes, J. I.; Villar-Rodil, S.; Guardia, L.; Solís-Fernández, P.; Salinas-Torres, D.; Cazorla-Amorós, D.; Morallón, E.; Martínez-Alonso, A.; Tascón, J. M. D. Investigating the Influence of Surfactants on the Stabilization of Aqueous Reduced Graphene Oxide Dispersions and the Characteristics of Their Composite Films. *Carbon* **2012**, *50*, 3184−3194.
(42) Dong, X.; Shi, Y.; Zhao, Y.; Chen, D.; Ye, J.; Yao, Y.; Gao, F.; Ni, Z.; Yu, T.; Shen, Z.; Huang, Y.; Chen, P.; Li, L.-J. Symmetry Breaking of Graphene Monolayers by Molecular Decoration. *Phys. Rev. Lett.* **2009**, *102*, 135501.
(43) Su, Q.; Pang, S.; Alijani, V.; Li, C.; Feng, X.; Müllen, K. Composites of Graphene with Large Aromatic Molecules. *Adv. Mater.* **2009**, *21*, 3191−3195.
(44) Zhang, M.; Parajuli, R. R.; Mastrogiovanni, D.; Dai, B.; Lo, P.; Cheung, W.; Brukh, R.; Chiu, P. L.; Zhou, T.; Liu, Z.; Garfunkel, E.; He, H. Production of Graphene Sheets by Direct Dispersion with Aromatic Healing Agents. *Small* **2010**, *6*, 1100−1107.
(45) Yang, H.; Hernandez, Y.; Schlierf, A.; Felten, A.; Eckmann, A.; Johal, S.; Louette, P.; Pireaux, J.-J.; Feng, X.; Mullen, K.; Palermo, V.; Casiraghi, C. A simple method for graphene production based on exfoliation of graphite in water using 1-pyrenesulfonic acid sodium salt. *Carbon* **2013**, *53*, 357−365.
(46) Schlierf, A.; Yang, H.; Gebremedhn, E.; Treossi, E.; Ortolani, L.; Chen, L.; Minoia, A.; Morandi, V.; Samorì, P.; Casiraghi, C.; Beljonne, D.; Palermo, V. Nanoscale Insight into the Exfoliation Mechanism of Graphene with Organic Dyes: Effect of Charge, Dipole and Molecular Structure. *Nanoscale* **2013**, *5*, 4205−4216.
(47) (a) Welsh, D. J.; O'Driscoll, L. J.; Bailey, S. W. D.; Visontai, D.; Howes, K.; Frampton, H.; Bryce, M. R.; Lambert, C. J. Key role of the linker in pyrene-linker-carboxylate surfactants for the efficient aqueous dispersion of multiwalled carbon nanotubes. *RSC Adv.* **2015**, *5*, 95360−95368. (b) Ernst, F.; Heek, T.; Setaro, A.; Haag, R.; Reich, S. Functional Surfactants for Carbon Nanotubes: Effects of Design. *J. Phys. Chem. C* **2013**, *117*, 1157−1162. (c) Setaro, A. Advanced carbon nanotubes functionalization. *J. Phys.: Condens. Matter* **2017**, *29*, 423003. (d) Zhang, N.; Zhou, D.; Zhou, N.; Zhang, Z.; Zhu, X. Dispersion of single-walled carbon nanotubes in an aqueous medium by using a cyclic copolymer. *React. Funct. Polym.* **2017**, *113*, 85−92. (e) Ernst, F.; Gao, Z.; Arenal, R.; Heek, T.; Setaro, A.; Fernandez-Pacheco, R.; Haag, R.; Cognet, L.; Reich, S. Noncovalent Stable Functionalization Makes Carbon Nanotubes Hydrophilic and Biocompatible. *J. Phys. Chem. C* **2017**, *121*, 18887−18891. (f) Mohamed, A.; Ardyani, T.; Abu Bakar, S.; Sagisaka, M.; Umetsu, Y.; Hamon, J. J.; Rahim, B. A.; Esa, S. R.; Abdul Khalil, H. P. S.; Mamat, M. H.; King, S.; Eastoe, J. Rational design of aromatic surfactants for graphene/natural rubber latex nanocomposites with enhanced electrical conductivity. *J. Colloid Interface Sci.* **2018**, *516*, 34−47.
(48) For a pertinent example see: Liscio, A.; Kouroupis-Agalou, K.; Kovtun, A.; Gebremedhn, E.; El Garah, M.; Rekab, W.; Orgiu, E.; Giorgini, L.; Samorì, P.; Beljonne, D.; Palermo, V. Exfoliation of Few-

DOI: 10.1021/acsomega.8b03147
ACS Omega 2019, 4, 1969−1981

Layer Graphene in Volatile Solvents Using Aromatic Perylene Diimide Derivatives as Surfactants. *ChemPlusChem* **2016**, *82*, 358−367.
(49) The prepation of compound PBSA was reported during the course of our investigation (see also ref 50): Yao, Z.; Qiao, Y.; Liang, H.; Ge, W.; Zhang, L.; Cao, Z.; Wu, H.-C. Approach Based on Polyelectrolyte-Induced Nanoassemblies for Enhancing Sensitivity of Pyrenyl Probes. *Anal. Chem.* **2016**, *88*, 10605−10610.
(50) Qiao, Y.; Yao, Z.; Ge, W.; Zhang, L.; Wu, H.-C. Rapid and Visual Detection of Heparin Based on the Disassembly of Polyelectrolyte-Induced Pyrene Excimers. *Org. Biomol. Chem.* **2017**, *15*, 2569−2574.
(51) Appel, R. Tertiary Phosphane/Tetrachloromethane, a Versatile Reagent for Chlorination, Dehydration, and P-N Linkage. *Angew. Chem., Int. Ed.* **1975**, *14*, 801−811.
(52) Ham, H.-W.; An, H.-C.; Han, J.-W.; Kim, G.-T.; Kim, D.-J. Light-Emitting Quantum Dots Having pH-Dependent Color Changing Capping Ligand. WO 2014077582 A1, 2014; PCT Int. Appl.
(53) See: Zaaba, N. I.; Foo, K. L.; Hashim, U.; Tan, S. J.; Liu, W.-W.; Voon, C. H. Synthesis of Graphene Oxide using Modified Hummers Method: Solvent Influence. *Procedia Eng.* **2017**, *184*, 469−477 and references therein .
(54) For an overview see: De Silva, K. K. H.; Huang, H.-H.; Joshi, R. K.; Yoshimura, M. Chemical reduction of Graphene Oxide Using Green Reductants. *Carbon* **2017**, *119*, 190−199.
(55) King, A. A. K.; Davies, B. R.; Noorbehesht, N.; Newman, P.; Church, T. L.; Harris, A. T.; Razal, J. M.; Minett, A. I. A New Raman Metric for the Characterisation of Graphene Oxide and Its Derivatives. *Sci. Rep.* **2016**, *6*, 19491.
(56) Ciesielski, A.; Samorì, P. Grapheneviasonication assisted liquid-phase exfoliation. *Chem. Soc. Rev.* **2014**, *43*, 381−398.
(57) Tao, H.; Zhang, Y.; Gao, Y.; Sun, Z.; Yan, C.; Texter, J. Scalable exfoliation and dispersion of two-dimensional materials - an update. *Phys. Chem. Chem. Phys.* **2017**, *19*, 921−960.
(58) For an example see: Ayán-Varela, M.; Paredes, J. I.; Guardia, L.; Villar-Rodil, S.; Munuera, J. M.; Díaz-González, M.; Fernández-Sánchez, C.; Martínez-Alonso, A.; Tascón, J. M. D. Achieving Extremely Concentrated Aqueous Dispersions of Graphene Flakes and Catalytically Efficient Graphene-Metal Nanoparticle Hybrids with Flavin Mononucleotide as a High-Performance Stabilizer. *ACS Appl. Mater. Interfaces* **2015**, *7*, 10293−10307.
(59) For an example see: Sun, Z.; Masa, J.; Liu, Z.; Schuhmann, W.; Muhler, M. Highly Concentrated Aqueous Dispersions of Graphene Exfoliated by Sodium Taurodeoxycholate: Dispersion Behavior and Potential Application as a Catalyst Support for the Oxygen-Reduction Reaction. *Chem.—Eur. J.* **2012**, *18*, 6972−6978.
(60) Stankovich, S.; Piner, R. D.; Chen, X.; Wu, N.; Nguyen, S. T.; Ruoff, R. S. Stable aqueous dispersions of graphitic nanoplatelets via the reduction of exfoliated graphite oxide in the presence of poly(sodium 4-styrenesulfonate). *J. Mater. Chem.* **2006**, *16*, 155−158.
(61) Konios, D.; Stylianakis, M. M.; Stratakis, E.; Kymakis, E. Dispersion behaviour of graphene oxide and reduced graphene oxide. *J. Colloid Interface Sci.* **2014**, *430*, 108−112.
(62) For a pertinent discussion see: Zhang, K.; Zhang, X.; Li, H.; Xing, X.; Jin, L.; Cao, Q.; Li, P. Direct Exfoliation of Graphite into Graphene in Aqueous Solution Using a Novel Surfactant Obtained from Used Engine Oil. *J. Mater. Sci.* **2017**, *53*, 2484−2496.
(63) (a) Arao, Y.; Mori, F.; Kubouchi, M. Efficient Solvent Systems For Improving Production of Few-Layer Graphene in Liquid Phase Exfoliation. *Carbon* **2017**, *118*, 18−24. (b) Parviz, D.; Irin, F.; Shah, S. A.; Das, S.; Sweeney, C. B.; Green, M. J. Challenges in Liquid-Phase Exfoliation, Processing, and Assembly of Pristine Graphene. *Adv. Mater.* **2016**, *28*, 8796−8818.
(64) Gayathri, S.; Jayabal, P.; Kottaisamy, M.; Ramakrishnan, V. Synthesis of Few Layer Graphene by Direct Exfoliation of Graphite and a Raman Spectroscopic Study. *AIP Adv.* **2014**, *4*, 027116.
(65) Ager, D.; Vasantha, V. A.; Crombez, R.; Texter, J. Aqueous Graphene Dispersions-Optical Properties and Stimuli-Responsive Phase Transfer. *ACS Nano* **2014**, *8*, 11191−11205.
(66) Backes, C.; Paton, K. R.; Hanlon, D.; Yuan, S.; Katsnelson, M. I.; Houston, J.; Smith, R. J.; McCloskey, D.; Donegan, J. F.; Coleman, J. N. Spectroscopic metrics allow in situ measurement of mean size and thickness of liquid-exfoliated few-layer graphene nanosheets. *Nanoscale* **2016**, *8*, 4311−4323.
(67) Eckmann, A.; Felten, A.; Mishchenko, A.; Britnell, L.; Krupke, R.; Novoselov, K. S.; Casiraghi, C. Probing the Nature of Defects in Graphene by Raman Spectroscopy. *Nano Lett.* **2012**, *12*, 3925−3930.
(68) Vincent, M. A.; Hillier, I. H. Accurate Prediction of Adsorption Energies on Graphene, Using a Dispersion-Corrected Semiempirical Method Including Solvation. *J. Chem. Inf. Model.* **2014**, *54*, 2255−2260.
(69) Groszek, A. J. Selective Adsorption at Graphite/Hydrocarbon Interfaces. *Proc. R. Soc. London, Ser. A* **1970**, *314*, 473−498.
(70) Olszak, T. A.; Willig, F.; Durfee, W. S.; Dreissig, W.; Bradaczek, H. Structure of 1-pyrenebutanoic acid. *Acta Crystallogr., Sect. C: Struct. Chem.* **1989**, *45*, 803−805.
(71) Rochefort, A.; Wuest, J. D. Interaction of Substituted Aromatic Compounds with Graphene. *Langmuir* **2009**, *25*, 210−215.
(72) Cai, X.; Wang, J.; Chi, R.; Song, Y.; Li, J.; Sun, Q.; Jia, Y. Direct Exfoliation of Graphite into Graphene by Pyrene-Based Molecules as Molecular-Level Wedges: A Tribological View. *Tribol. Lett.* **2016**, *62*, 1−8.
(73) For the use of other amphiphilic exfoliants see: Kabe, R.; Feng, X.; Adachi, C.; Müllen, K. Exfoliation of Graphite into Graphene in Polar Solvents Mediated by Amphiphilic Hexa-peri-hexabenzocoronene. *Chem.—Asian J.* **2014**, *9*, 3125−3129.
(74) Menger, F. M.; Whitesell, L. G. Binding Properties of 1-Pyrenesulfonic Acid in Water. *J. Org. Chem.* **1987**, *52*, 3793−3798.
(75) Varenik, M.; Green, M. J.; Regev, O. Distinguishing Self-Assembled Pyrene Structures from Exfoliated Graphene. *Langmuir* **2016**, *32*, 10699−10704.
(76) Bailey, S.; Visontai, D.; Lambert, C. J.; Bryce, M. R.; Frampton, H.; Chappell, D. A Study of Planar Anchor Groups for Graphene-Based Single-Molecule Electronics. *J. Chem. Phys.* **2014**, *140*, 054708.
(77) Emery, J. D.; Wang, Q. H.; Zarrouati, M.; Fenter, P.; Hersam, M. C.; Bedzyk, M. J. Structural analysis of PTCDA monolayers on epitaxial graphene with ultra-high vacuum scanning tunneling microscopy and high-resolution X-ray reflectivity. *Surf. Sci.* **2011**, *605*, 1685−1693.
(78) Zhen, X. V.; Swanson, E. G.; Nelson, J. T.; Zhang, Y.; Su, Q.; Koester, S. J.; Bühlmann, P. Noncovalent Monolayer Modification of Graphene Using Pyrene and Cyclodextrin Receptors for Chemical Sensing. *ACS Appl. Nano Mater.* **2018**, *1*, 2718−2726.
(79) Pathipati, S. R.; Pavlica, E.; Treossi, E.; Rizzoli, R.; Veronese, G. P.; Palermo, V.; Chen, L.; Beljonne, D.; Cai, J.; Fasel, R.; Ruffieux, P.; Bratina, G. Modulation of charge transport properties of reduced graphene oxide by submonolayer physisorption of an organic dye. *Org. Electron.* **2013**, *14*, 1787−1792.
(80) Backes, C.; Hauke, F.; Hirsch, A. Tuning the adsorption of perylene-based surfactants on the surface of single-walled carbon nanotubes. *Phys. Status Solidi B* **2013**, *250*, 2592−2598.
(81) Bartlam, C.; Morsch, S.; Heard, K. W. J.; Quayle, P.; Yeates, S. G.; Vijayaraghavan, A. Nanoscale infrared identification and mapping of chemical functional groups on graphene. *Carbon* **2018**, *139*, 317−324.
(82) Rourke, J. P.; Pandey, P. A.; Moore, J. J.; Bates, M.; Kinloch, I. A.; Young, R. J.; Wilson, N. R. The Real Graphene Oxide Revealed: Stripping the Oxidative Debris from the Graphene-like Sheets. *Angew. Chem., Int. Ed.* **2011**, *50*, 3173−3177.
(83) Van Der Spoel, D.; Lindahl, E.; Hess, B.; Groenhof, G.; Mark, A. E.; Berendsen, H. J. C. GROMACS: Fast, flexible, and free. *J. Comput. Chem.* **2005**, *26*, 1701−1718.
(84) Nosé, S. A Molecular Dynamics Method for Simulations in the Canonical Ensemble. *Mol. Phys.* **2006**, *52*, 255−268.

DOI: 10.1021/acsomega.8b03147
ACS Omega 2019, 4, 1969−1981

(85) Hoover, W. G. Canonical dynamics: equilibrium phase-space distributions. *Phys. Rev. A: At., Mol., Opt. Phys.* **1985**, *31*, 1695−1697.
(86) MacKerell, A. D.; Bashford, D.; Bellott, M.; Dunbrack, R. L.; Evanseck, J. D.; Field, M. J.; Fischer, S.; Gao, J.; Guo, H.; Ha, S.; Joseph-McCarthy, D.; Kuchnir, L.; Kuczera, K.; Lau, F. T. K.; Mattos, C.; Michnick, S.; Ngo, T.; Nguyen, D. T.; Prodhom, B.; Reiher, W. E.; Roux, B.; Schlenkrich, M.; Smith, J. C.; Stote, R.; Straub, J.; Watanabe, M.; Wiórkiewicz-Kuczera, J.; Yin, D.; Karplus, M. All-Atom Empirical Potential for Molecular Modeling and Dynamics Studies of Proteins. *J. Phys. Chem. B* **1998**, *102*, 3586−3616.
(87) Kramer, C.; Gedeck, P.; Meuwly, M. Multipole-Based Force Fields from ab Initio Interaction Energies and the Need for Jointly Refitting All Intermolecular Parameters. *J. Chem. Theory Comput.* **2013**, *9*, 1499−1511.
(88) Vanommeslaeghe, K.; Hatcher, E.; Acharya, C.; Kundu, S.; Zhong, S.; Shim, J.; Darian, E.; Guvench, O.; Lopes, P.; Vorobyov, I.; MacKerell, A. D. CHARMM General Force Field: A Force Field for Drug-Like Molecules Compatible with the CHARMM All-Atom Additive Biological Force Fields. *J. Comput. Chem.* **2010**, *31*, 671−690.
(89) Joung, I. S.; Cheatham, T. E., III. Determination of Alkali and Halide Monovalent Ion Parameters for Use in Explicitly Solvated Biomolecular Simulations. *J. Phys. Chem. B* **2008**, *112*, 9020−9041.
(90) Jorgensen, W. L.; Chandrasekhar, J.; Madura, J. D.; Impey, R. W.; Klein, M. L. Comparison Of Simple Potential Functions For Simulating Liquid Water. *J. Chem. Phys.* **1983**, *79*, 926−935.
(91) Darden, T.; York, D.; Pedersen, L. Particle mesh Ewald: An N·log(N) method for Ewald sums in large systems. *J. Chem. Phys.* **1993**, *98*, 10089−10092.
(92) Essmann, U.; Perera, L.; Berkowitz, M. L.; Darden, T.; Lee, H.; Pedersen, L. G. A Smooth Particle Mesh Ewald Method. *J. Chem. Phys.* **1995**, *103*, 8577−8593.
(93) Torrie, G. M.; Valleau, J. P. Monte Carlo free energy estimates using non-Boltzmann sampling: Application to the sub-critical Lennard-Jones fluid. *Chem. Phys. Lett.* **1974**, *28*, 578−581.
(94) Torrie, G. M.; Valleau, J. P. Nonphysical sampling distributions in Monte Carlo free-energy estimation: Umbrella sampling. *J. Comput. Phys.* **1977**, *23*, 187−199.
(95) Kumar, S.; Rosenberg, J. M.; Bouzida, D.; Swendsen, R. H.; Kollman, P. A. THE weighted histogram analysis method for free-energy calculations on biomolecules. I. The method. *J. Comput. Chem.* **1992**, *13*, 1011−1021.
(96) Hub, J. S.; de Groot, B. L.; van der Spoel, D. g_wham-A Free Weighted Histogram Analysis Implementation Including Robust Error and Autocorrelation Estimates. *J. Chem. Theory Comput.* **2010**, *6*, 3713−3720.
(97) Řezáč, J.; Fanfrlík, J.; Salahub, D.; Hobza, P. Semiempirical Quantum Chemical PM6 Method Augmented by Dispersion and H-Bonding Correction Terms Reliably Describes Various Types of Noncovalent Complexes. *J. Chem. Theory Comput.* **2009**, *5*, 1749−1760.
(98) Stewart, J. J. P. *MOPAC2012*; Stewart Computational Chemistry: Colorado Springs, CO, 2012.

DOI: 10.1021/acsomega.8b03147
ACS Omega 2019, 4, 1969−1981